View metadata, citation and similar papers at core.ac.uk
brought to you by CORE
provided by DigitalCommons@USU

THERMAL TRANSPORT TO DROPLETS IMPINGING ON HEATED, SUPERHYDROPHOBIC SURFACES

Jonathan C. Burnett
Department of Mechanical Engineering
Brigham Young University
Provo, Utah 84602

Dan Maynes*
Julie Crockett
Department of Mechanical Engineering
Brigham Young University
Provo, Utah, 84602

ABSTRACT

An analytical model is developed to quantify the heat transfer to droplets impinging on heated superhydrophobic surfaces. Integral analysis is used to incorporate the apparent temperature jump at the superhydrophobic surface as a boundary condition. This model is combined with a fluid model which incorporates velocity slip to calculate the cooling effectiveness, a metric outlined in contemporary work. The effect of varying velocity slip and temperature jump is analyzed for different impact Weber numbers and contact angles for surface temperatures below 100 °C. Heat transfer to the drop on superhydrophobic surfaces is decreased when compared to conventional surfaces.

INTRODUCTION

Heat transfer to impinging droplets is a scenario which is encountered in a wide range of applications. A better understanding of the process has potential impact on spray cooling applications, understanding ice formation (particularly on aircraft), fuel injection, and inkjet printing for several examples. The highly transient nature of the process combined with very short timescales, however, makes it a complex, difficult problem to understand and model.

Superhydrophobic (SH) surfaces have been a topic of recent increased study due to their unique properties which impact and often significantly change the hydrodynamic and heat transfer behavior of these surfaces. With potential applications for SH surfaces in self-cleaning surfaces, condensers, and anti-icing surfaces, an understanding of how the heat transfer changes for impinging droplets on a SH surface is desired.

Previous analytical work exploring the heat transfer to impinging drops on standard, smooth surfaces either do so by using a computer simulation, typically via a Volume-of-Fluid (VOF) approach [1, 2], or develop a more simplified analytical model which captures the overall heat transfer to the droplet [3–5]. The computer models are a good point of comparison for analytical models and resolve the entire velocity and temperature profile inside the drop but are typically limited in range of parameters presented and require significant computation time for each case run. When only the overall heat transfer is required then an analytical model can satisfy any design requirements without needing the high computation and time costs.

No previous work exists which models the heat transfer to impinging drops on a SH surface larger than micro-scale for a wide range of impact conditions. This work outlines an analytical model which will approximate the heat transfer to an impinging drop on a SH surface.

BACKGROUND

When a water drop comes in contact with a surface it forms an angle that is determined by the surface energy of the material. The surface is denoted either hydrophilic ('wetting') or hydrophobic ('non-wetting') depending on if this angle is greater or less than 90°. When the contact angle exceeds 150°, however, the surface is defined as superhydrophobic.

SH surfaces create this high contact angle via a micro/nano-structured surface (typically a post or rib pattern for lab-made surfaces) covered in a hydrophobic coating. Due to the small nature of the cavities between this structure, the hydrophobic coating causes the surface tension of the water to prevent it from entering the cavities. This significantly decreases the contact

*Address all correspondence to this author.

area the droplet has with the surface, and is the primary cause of the deviation of behavior from that of typical surfaces. SH surfaces are defined and distinguished from one another primarily by three parameters: The cavity fraction, F_c, which is the percentage of frontal area of a surface which is cavities; the pitch, which is the distance between identical surface features (left edge of one rib to the next, for example); and the feature height. Cavity fractions of typical SH surfaces can range from anywhere between 80% to mid-90%. This over 80% reduction of contact area in a drop causes the enhanced droplet mobility as well as greatly decreases the heat transfer to drops suspended on the surface.

Engineered SH surfaces with a repeating pattern have particularly unique hydrodynamic characteristics. Wherever the water is over a cavity an approximate free-shear boundary condition exists which allows the fluid to move. A slip-velocity at the wall can be defined to quantify this effect averaged on the macroscale. This is expressed using the slip model proposed by Navier as

$$u_s = \lambda \left(\frac{\partial u}{\partial n} \right)_{wall} \tag{1}$$

where u_s is the aggregate slip velocity and λ is what's defined as the slip length [6]. Physically this length can be interpreted as the distance into the wall that the velocity profile would need to be extrapolated to reach the no-slip condition. This is a useful model as the slip length for a wide range of surface structure variants has been modeled. For a post surface, Ybert *et al.* outlined a model for the slip length as a function of the cavity fraction as

$$\frac{\lambda}{L} = \frac{0.325}{\sqrt{1-F_c}} - 0.44 \tag{2}$$

where L is the pitch and F_c is the cavity fraction and is valid for $70\% \leq F_c \leq 98\%$. This average slip velocity has significant drag reduction effects and impacts the overall contact time of an impinging droplet on the surface. Similarly, for the heat transfer on a SH surface, the insulating behavior of the air cavities greatly reduces the heat transfer expected and is expressed on a macro level as an average temperature jump at the wall by

$$\Delta T_w = \lambda_T \left(\frac{\partial T}{\partial n} \right)_{wall} \tag{3}$$

where ΔT_w is the average temperature jump at the wall due to the air insulation, λ_T is the temperature jump length, and $\frac{\partial T}{\partial n}$ is the temperature gradient normal to the wall.

Previous analytical models for impinging droplets on smooth surfaces predict the overall heat transfer without resolving the entire temperature profile for the entire drop. Pasandideh-fard *et al.* in 2000 proposed a non-dimensional term which captures the overall heat transfer well called cooling effectiveness and defined it as [3]

$$\varepsilon(t) = \frac{\int_0^t \int_{A_c} q''(t)\, dA_c dt}{mc_p\,(T_w - T_{dr})} \tag{4}$$

where ε is the cooling effectiveness, $q''(t)$ is the heat flux at the wall, A_c is the contact area of the drop, m is the mass of the drop, c_p is the specific heat of the liquid, and T_w and T_{dr} is the wall and initial droplet temperature respectively. Strotos *et al.* created a semi-analytical model by expressing $q''(t)$ as proportional to the heat flux for one-dimensional heat transfer between two semi-infinite media [4]. After finding the proportionality constant by comparison to their own VOF model, they integrated using contact area data from a VOF model resulting in a semi-analytical estimation of the cooling effectiveness. They later improved their model by removing the reliance on a proportionality constant by using the heat flux developed by Roisman *et al.* for their similarity solution [7]. This heat flux expression was again integrated using the contact area data from their VOF model [5].

The current work contributes and expands on this previous work by developing an analytical model which can be applied to SH surfaces in addition to conventional, smooth surfaces. The work also analyzes four prior work's velocity profiles from hydrodynamic models for their effectiveness in capturing the convection effects of an impinging droplet. Upon selection of the most effective velocity profile, the total heat transfer model is then used to quantify the effect of temperature jump length, contact angle, and Weber number on the overall heat transfer. This provides an analytical framework for modeling droplet impingement heat transfer to SH surfaces.

1 Methodology

To model the heat transfer to the droplet both the hydrodynamics (to obtain the contact area) and the heat flux at the wall have to be modeled. The hydrodynamic model developed by Clavijo *et al.* for droplet impingement on SH surfaces will be used and is summarized here [8].

1.1 Hydrodynamic Model

A range of approaches have been used to model the hydrodynamics of impinging droplets. Computer models often use the Volume-of-Fluid (VOF) method which models the entirety of the droplet during the impingement process [1,2]. Analytical models often simplify the problem via assumptions to obtain the contact area of the drop. Attane *et al.* developed an analytical model to predict the diameter of the drop as a function of time by balancing the kinetic energy, surface energy, and viscous dissipation of

the drop [9]. They explored several shapes and associated velocity profiles for the droplet control volume, settling on a cylindrical control volume which flattens over time as the most accurate. The resulting diameter as a function of time is a good fit to experimental values for a wide range of Weber numbers and contact angles.

Clavijo *et al.* expanded on this work by adding slip to the assumed velocity profile and energy equation [8]. Their results matched well with experiments conducted for a wide range of Weber numbers and slip lengths. The velocity profile with added slip is

$$\vec{V} = \begin{bmatrix} Cr(z+\lambda) \\ -C(z^2+2\lambda z) \end{bmatrix} \tag{5}$$

where z is the height above the surface and the constant C is obtained by ensuring the average velocity at the outer radius of the droplet is equal to the expansion rate of the drop. The resulting differential equation then becomes

$$\begin{aligned} &\frac{d}{d\hat{t}}\left[\hat{R}^2(1-cos\Theta)+\frac{1}{3\hat{R}}\right] \\ &+\frac{1}{3888}\frac{d}{d\hat{t}}\left[\frac{1}{\hat{R}^{10}}\left(2\hat{\lambda}+\frac{1}{6\hat{R}^2}\right)^{-2}\left(\frac{d\hat{R}}{d\hat{t}}\right)^2\left(6\hat{R}^6\right.\right. \\ &\left.\left.+108\hat{\lambda}\hat{R}^8+648\hat{\lambda}^2\hat{R}^{10}+\frac{1}{5}+6\hat{\lambda}\hat{R}^2+48\hat{\lambda}^2\hat{R}^7\right)\right] \\ &+\frac{Oh}{3}\left(\hat{\lambda}+\frac{1}{12\hat{R}^2}\right)^{-2}\left(\frac{1}{18\hat{R}^6}+\frac{\hat{\lambda}}{\hat{R}^4}\right. \\ &\left.+\frac{6\hat{\lambda}^2}{\hat{R}^2}+\frac{1}{4}+\frac{s}{12\hat{R}^3}\right)\left(\frac{d\hat{R}}{d\hat{t}}\right)^2=0 \end{aligned} \tag{6}$$

where $s = 1.41Oh^{-2/3}$, $\hat{R} = R/D_0$, $\hat{\lambda} = \lambda/D_0$, and $\hat{t} = tV_0/\left(D_0\sqrt{We}\right)$, and D_0 is the diameter of the droplet before impingement. Two boundary conditions are necessary to solve this problem. The first is found by ensuring that the initial surface energy of the cylindrical control volume is the same as the surface energy of the spherical droplet. The second is done by ensuring the kinetic energies of the two droplets are equal. This yields

$$\frac{d\hat{R}_0}{d\hat{t}} = \frac{\left(2\hat{\lambda}+\hat{R}_0^2/6\right)\sqrt{324\hat{R}_0^{10}We}}{\sqrt{6\hat{R}_0^6+108\hat{\lambda}\hat{R}_0^8+648\hat{\lambda}^2\hat{R}_0^10+0.2+6\hat{\lambda}\hat{R}_0^2+48\hat{\lambda}^2\hat{R}_0^7}} \tag{7}$$

The predicted diameter as a function of time was compared to experiments with good results. For the heat transfer model the total contact time needs to be estimated. Using the approach outlined by Guo *et al.* [10] this is expressed by

$$t_c = \frac{\pi}{2\sqrt{2(1-\cos\theta_{CB})}}\sqrt{\frac{\rho D_0^3}{\gamma}} \tag{8}$$

where γ is the surface tension of the liquid and θ_{CB} is the Cassie-Baxter contact angle given by $\cos\theta_{CB} = (1-f_c)\cos\theta_0 - 1$.

Clavijo et *al.* also details the use of the model for anistropic slip. The slip can be modeled on an anisotropic ribbed surface by Lauga and Stone for scenarios where the ribs are aligned both parallel and perpendicular to the flow direction. These are respectively expressed as

$$\left(\frac{\lambda}{w}\right)_{\parallel} = \frac{1}{\pi}\ln\left(\sec\left(\frac{F_c\pi}{2}\right)\right) \tag{9}$$

and

$$\left(\frac{\lambda}{w}\right)_{\perp} = \frac{1}{2\pi}\ln\left(\sec\left(\frac{F_c\pi}{2}\right)\right) \tag{10}$$

where $\parallel$ and $\perp$ refer to parallel and perpendicular respectively, λ is again the hydrodynamic slip length, w is the module width of a repeating cavity and rib, and F_c is the cavity fraction, w_c/w, where w_c is the cavity width [11]. For the flow scenario of droplet impingement, a continuous expression is needed for the slip length as it varies with inclination angle from the parallel rib direction. Crowdy expanded on the work of Lauga and Stone and proposed an expression for the slip length as it varies with direction as

$$\lambda(\phi) = \lambda_{\parallel}\sqrt{\cos^2\phi+\left(\frac{\sin\phi}{2}\right)^2} \tag{11}$$

where ϕ is the angle between the direction of the ribs and the flow direction considered [12]. Using this expression for slip, Clavijo et *al.* split a 90° section of the drop into 252 angular wedges and calculated the expansion of the drop independently, ensuring the height across the drop was the same at each time-step by enforcing constant volume. This expanded hydrodynamic model is used to model the surface area of the droplet over time for SH surfaces with anisotropic slip.

1.2 Heat Transfer Model

Previous analytical models for heat transfer to impinging drops on smooth surfaces have modeled the heat flux either by

comparison to a VOF model or by using a similarity solution to estimate the heat flux. Neither of these approaches can be applied to cases with slip at the wall, and so a new method needs to be developed. One potential approach is outlined by Searle *et al.* in their work on heat transfer to an impinging jet on a SH surface [13]. They implemented an integral method to develop a differential equation to predict the heat flux into the jet. A similar approach will be used to model the heat flux for the impinging droplet by starting with an assumed quadratic temperature profile with the boundary conditions

$$T(z=0) = T_c - \Delta T_w \tag{12}$$

$$T(z=\delta_T) = T_{dr} \tag{13}$$

$$\frac{\partial T}{\partial t}(z=0) = 0 \tag{14}$$

where δ_T is an approximate thermal boundary layer height and T_c is the contact temperature found for two contacting semi-infinite media by

$$T_c = \frac{e_{liq}T_d + e_{sol}T_w}{e_{liq} + e_{sol}} \tag{15}$$

where e_{sol} and e_{liq} is the thermal effusivity of the wall and droplet respectively. Using the boundary conditions and the definition of temperature jump length to simplify yields

$$T(z,t) = T_c - \frac{2\lambda_T(T_c - T_{dr})}{2\lambda_T + \delta_T} - \frac{2(T_c - T_{dr})}{2\lambda_T + \delta_T}z + \frac{T_c - T_{dr}}{\delta_T(2\lambda_T + \delta_T)}z^2 \tag{16}$$

Applying Fourier's law gives the heat flux as

$$q_w'' = \frac{2k(T_c - T_{dr})}{2\lambda_T + \delta_T} \tag{17}$$

To resolve the heat flux an expression for the thermal boundary layer height is needed. To obtain this the integral method is applied to the convection-diffusion equation. By assuming the drop is axisymmetric and that, near the wall, $\frac{\partial T}{\partial r} << \frac{\partial T}{\partial z}$ the convection-diffusion equation becomes

$$\frac{\partial T}{\partial t} + u_z\frac{\partial T}{\partial z} = \alpha\frac{\partial^2 T}{\partial z^2} \tag{18}$$

where α is the thermal diffusivity of the liquid. Integrating in z using the assumed temperature profile and simplifying yields

$$\alpha\frac{2(T_c - T_{dr})}{2\lambda_T + \delta_T} - \int_0^{\delta_T} u_z\frac{dT}{dz} = \left(\frac{2\delta_T(T_c - T_{dr})}{3(2\lambda_T + \delta_T)} - \frac{\delta_T^2(T_c - T_d)}{3(2\lambda_T + \delta_T)^2}\right)\frac{\partial \delta_T}{\partial t} \tag{19}$$

The integral term is dependent on the velocity profile used to capture the convection effects. Four different potential velocity fields will be considered to evaluate the integral. These four models will then be compared to prior models and experimental results on smooth surfaces to evaluate the goodness of each velocity profile in capturing the heat transfer of the droplet.

First, using the velocity profile from the hydrodynamic model defined in eq. 5, the remaining convection term becomes

$$\int_0^{\delta_T} u_z\frac{dT}{dz} = \frac{2}{R(H+2\lambda)}\frac{dR}{dt}\frac{(T_c - T_{dr})}{3(2\lambda_T + \delta_T)}\delta_T^2\left(\frac{1}{4}\delta_T + \lambda\right) \tag{20}$$

Second, a linear profile is evaluated, which assumes a uniform-in-z profile which varies linearly with r. Ensuring the velocity at the outer radius is the same as the expansion rate of the drop yields

$$U = \begin{bmatrix} u_r \\ u_z \end{bmatrix} = \begin{bmatrix} \frac{r}{R}\frac{dR}{dt} \\ -2\frac{1}{R}\frac{dR}{dt}z \end{bmatrix} \tag{21}$$

where R is the outer radius of the drop. Using this profile the convection term becomes

$$\int_0^{\delta_T} u_z\frac{dT}{dz} = \frac{2}{3}\frac{\delta_T^2(T_c - T_{dr})}{R(2\lambda_T + \delta_T)}\frac{dR}{dt} \tag{22}$$

The third profile evaluated is an inviscid flow profile used in other drop impingement models [7, 10], which is

$$U = \begin{bmatrix} u_r \\ u_z \end{bmatrix} = \begin{bmatrix} \frac{r}{t} \\ -\frac{2z}{t} \end{bmatrix} \tag{23}$$

Using this profile the convection term becomes

$$\int_0^{\delta_T} u_z\frac{dT}{dz} = \frac{2}{3}\frac{\delta_T^2}{t}\frac{(T_c - T_{dr})}{(2\lambda_T + \delta_T)} \tag{24}$$

This profile is unique when compared to the prior two in that the resulting equation is an explicit function of t and has no dependence on $\frac{dR}{dt}$. This means that for the no-slip case this has an exact solution of

$$\delta_T = \sqrt{\frac{12}{5}\alpha t} \tag{25}$$

The fourth and final velocity profile is outlined by Roisman *et al.* and is similar to the inviscid profile described above but has a constant which varies with impact condition. This profile is

$$U = \begin{bmatrix} u_r \\ u_z \end{bmatrix} = \begin{bmatrix} \frac{r}{t+c} \\ -\frac{2z}{t+c} \end{bmatrix} \tag{26}$$

The convection term using this equation is

$$\int_0^{\delta_T} u_z \frac{dT}{dz} = \frac{2}{3} \frac{\delta_T^2}{t+c} \frac{(T_c - T_{dr})}{(2\lambda_T + \delta_T)} \tag{27}$$

The resulting convection-diffusion equation is also only a function of time, and so the exact solution can be derived for the no-slip case as

$$\delta_T = \sqrt{\frac{12}{5}} \alpha \frac{\sqrt{(t+c)^5 - c^5}}{(t+c)^2} \tag{28}$$

The method used to expand the hydrodynamic model to incorporate anisotropic slip will also be used to expand the previously developed heat transfer model to apply to anisotropic cases. The wedge control volumes used in the hydrodynamic model can also be used to model the heat flux across the droplet. The angular difference in temperature jump length, however, introduces the possibility of needing to account for angular diffusion or advection. Re-examining the convection-diffusion equation in polar coordinates and simplifying by assuming (similar to the isotropic model) that, near the wall, $\frac{\partial T}{\partial r} << \frac{\partial T}{\partial z}$, the convection-diffusion becomes

$$\frac{\partial T}{\partial t} + \frac{u_\theta}{r} \frac{\partial T}{\partial \theta} + u_z \frac{\partial T}{\partial z} = \alpha \left(\frac{1}{r^2} \frac{\partial^2 T}{\partial \theta^2} \frac{\partial^2 T}{\partial z^2} \right) \tag{29}$$

A scaling analysis was performed to ascertain the relative impact that angular convection would have on the model if included. This was done by running the model for anisotropic slip assuming negligible angular convection and then using the resulting predicted temperature profile to evaluate the scaling ratio between angular and vertical advection and diffusion, or

$$\frac{u_\theta}{u_z} \frac{1}{r} \frac{\frac{\partial T}{\partial \theta}}{\frac{\partial T}{\partial z}}, \frac{1}{r^2} \frac{\frac{\partial^2 T}{\partial \theta^2}}{\frac{\partial^2 T}{\partial z^2}} \tag{30}$$

Since u_θ / u_z will be less than unity and neglecting angular convection will produce a larger gradient in the angular direction than will occur in unity, evaluating the ratios of these derivatives across the droplet will produce a good worse-case estimation of the scales of impact that angular advection and diffusion would have on heat transfer. This scale analysis showed that angular advection is less than 1% magnitude throughout the entirety of the droplet. Due to the presenence of $1/r^2$ in the diffusion comparison the impact of angular diffusion in comparison to vertical diffusion does become significant for very small radial locations. The overall effect, however, only exceeds a 1% magnitude of effect in less than 1% of the total volume of the drop over the entire spreading period. For this reason the assumption that angular convection can be neglected for anisotropic slip cases is a good assumption that will have minimal impact on the predicted cooling effectiveness. Thus a similar wedge control-volume approach will be used to evaluate the cooling effectiveness for anistropic surfaces.

2 Results

The four variations of the model using the different velocity profiles were compared to two previous models for no-slip surfaces. Pasandideh-fard *et al.* developed an analytical model which predicted the cooling effectiveness of a drop at the time of maximum expansion. They published a comparison of this model to a VOF model they developed for a variety of impact conditions. The same cases were run using the four variations of the slip model and are tabulated for comparison in Table 1.

Strotos *et al.* developed an analytical model for a no-slip case and compared their model to a previously developed VOF model [4], but normalized the cooling effectiveness by the contact temperature instead of the wall temperature. The cases they considered, however, had a dramatic difference in advancing and receding contact angle. Since the Clavijo *et al.* hydrodynamic model used here is unable to adjust the contact angle for retraction, the developed model can only be compared to the Strotos VOF model during expansion.

The cooling effectiveness, ε, is plotted vs time in Figure 1 for the Strotos VOF model, the Strotos semi-analytical model, and the developed model using the four different velocity profiles. The results demonstrate that the ε results derived using the Roisman velocity profile best matches the results of the VOF model. The ε results using the inviscid and linear profiles over and under predict the cooling effectiveness respectively. The linear profile, although matching well during expansion, begins to deviate from expected behavior during retraction as the assumed convection profile begins to significantly decrease the expected heat transfer due to the positive vertical velocity predicted. Interestingly the Clavijo profile, while accurate when used for the hydrodynamic model, severely under-predicts the cooling effectiveness when used in the convection term of the energy equation. Consequently only the Roisman velocity field model will be used to evaluate the effect of contact angle, temperature jump

TABLE 1. Comparison between Pasandideh-Fard VOF model and analytical model to the four variations of developed model.

Case	D_0	V_0	Re	We	$\varepsilon(t_{max})$ (VOF)	$\varepsilon(t_{max})$ (Analytical)	$\varepsilon(t_{max})$ (Clavijo)	$\varepsilon(t_{max})$ (Linear)	$\varepsilon(t_{max})$ (Inviscid)	$\varepsilon(t_{max})$ (Roisman)
1	2.0	1.3	2908	47	0.097	0.106	0.035	0.056	0.078	0.073
2	2.0	2.0	4474	111	0.115	0.105	0.053	0.087	0.115	0.098
3	2.0	3.0	6711	249	0.131	0.120	0.078	0.129	0.168	0.133
4	2.0	4.0	8948	443	0.140	0.125	0.101	0.166	0.215	0.158
5	0.5	1.3	727	12	0.102	0.088	0.028	0.041	0.064	0.062
6	0.5	2.0	1118	28	0.108	0.098	0.036	0.056	0.082	0.079
7	0.5	3.0	1678	62	0.119	0.131	0.049	0.079	0.110	0.092
8	0.5	4.0	2237	111	0.129	0.136	0.063	0.102	0.139	0.109

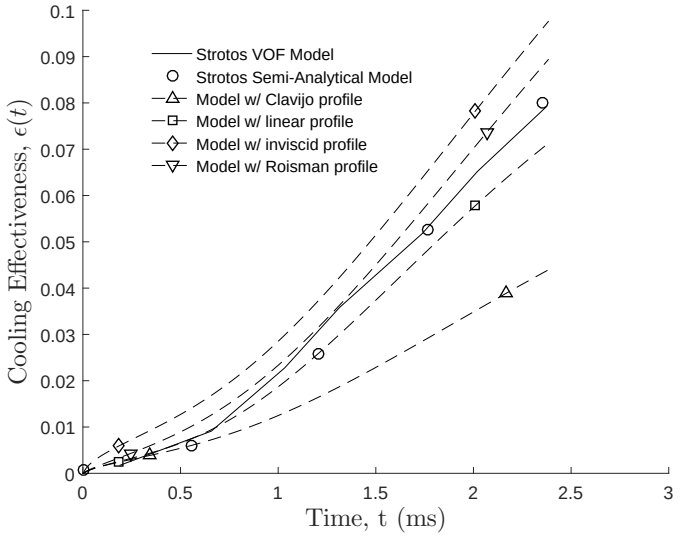

FIGURE 1. Cooling Effectiveness comparing to Strotos VOF model for the reference case vs the four velocity profile models.

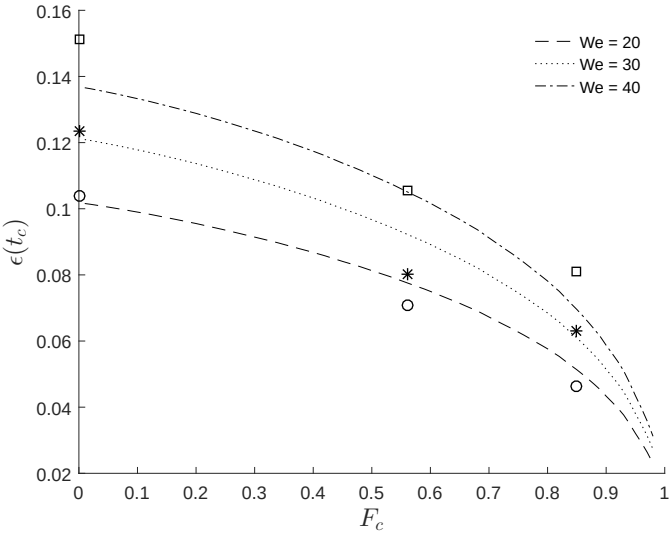

FIGURE 2. Comparison of cooling effectiveness after total contact time to experimental results from Chunfang *et al.* for various Weber numbers.

length, and Weber number on the total cooling effectiveness for an impinging droplet.

2.1 Comparison to Previous Experimental Results

Guo *et al.* found the total cooling effectiveness after rebound for various post SH surfaces [10]. For accurate comparison of the model to the results, all parameters needed to be matched. Weber, initial diameter, and fluid properties were able to be matched across cases. To match the slip and temperature jump lengths for the range of cavity fractions the slip outlined by Cowley *et al.* was used [14]. The contact angle was calculated using the general shape outlined by Cassie-Baxter as

$$cos(\theta) = (1 - F_c)cos\left(\theta^0\right) - F_c \tag{31}$$

where θ^0 is the contact angle on a smooth hydrophobic surface. This shape was scaled to match the experimentally obtained contact angles listed by Guo *et al.* for the surfaces used. The model then was run for varying cavity fractions and compared to the experimental results and is displayed in Fig. 2.

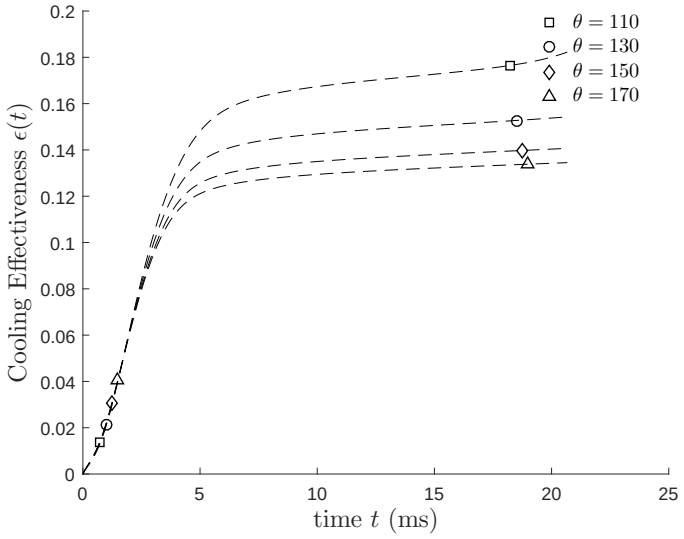

FIGURE 3. Cooling Effectiveness over time for a range of contact angles. The Weber number was 50 for all cases shown.

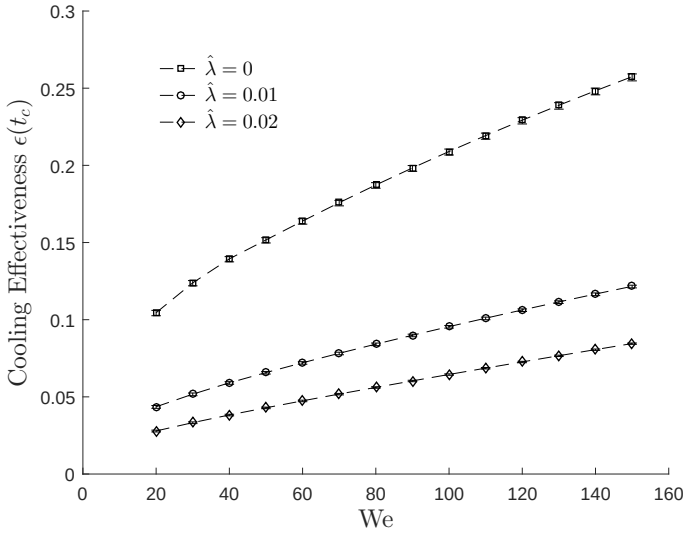

FIGURE 4. Sensitivity study for effect of contact time estimation. The upper and lower bounds were for a 10% increase and decrease in the estimated contact time.

2.2 Effect of Slip

The cooling effectiveness as a function of time for a no-slip case, with a Weber number of 50, for different contact angles is presented in Fig. 3. It's apparent that contact angle has little impact on the heat transfer during expansion, but has a notable impact during retraction. This also illustrates that by the time of droplet rebound the heat transfer has become negligible and so the total cooling efffectiveness after the contact time is not sensitive to the contact time estimation. To confirm this assumption a sensitivity study was run for varying slip length and Weber number by varying the estimated contact time by 10%. This is plotted with associated error bars in Fig. 4. This shows that the accuracy of the estimated contact time has little effect on the results.

The model was then exercised while holding contact angle at a constant 120° for various Weber numbers while varying slip length. For all cases the temperature jump length was assumed to be equal to the slip length. The cooling effectiveness after the total contact time vs normalized slip length is presented in Fig. 5. As expected these results demonstrate a notable decrease in heat transfer as slip increases for all Weber numbers. This is consistent with preliminary results as seen by Hays *et al.* for sessile droplets [15].

The impact of Weber number was studied by holding the contact angle constant at 120° for various slip lengths while varying the Weber number. The cooling effectiveness vs Weber number is presented in Fig. 6. The cooling effectiveness increases with increasing Weber number, as expected. The linearity of the trend seems to be largely unaffected by slip length.

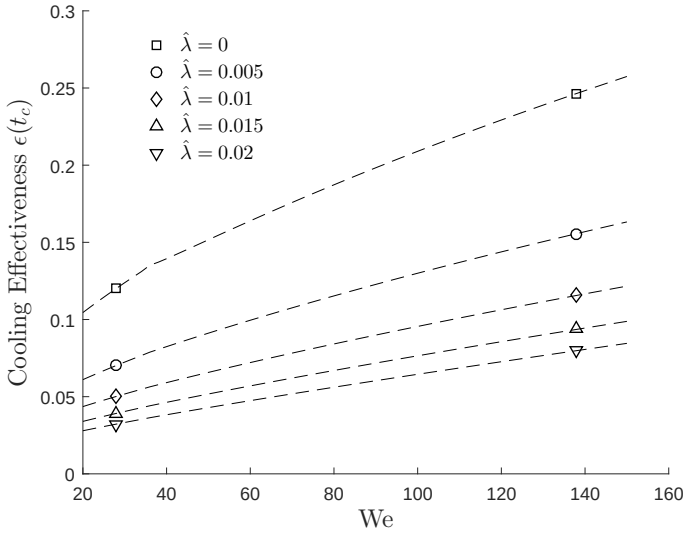

FIGURE 5. Total Cooling Effectiveness compared to the nondimensionalized slip length for a range of Weber numbers. The contact angle was 120 degrees for all cases shown.

2.3 Anisotropic SH Surfaces

Due to the simpler nature of the isotropic model over the anisotropic it is advantageous to use the isotropic model whenever possible. Thus, comparing the anisotropic model to see how its behavior deviates from the isotropic model is useful. When comparing the results between an isotropic and anisotropic SH

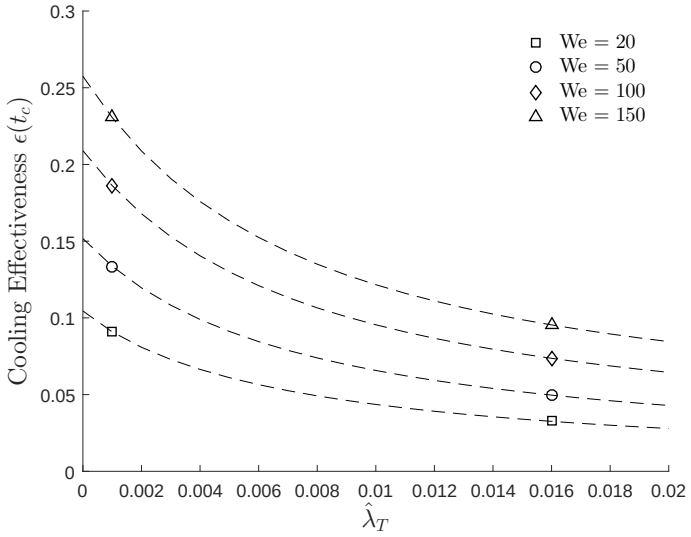

FIGURE 6. Total Cooling Effectiveness compared to the Weber number for a range of slip lengths. The contact angle was 120 degrees for all cases shown.

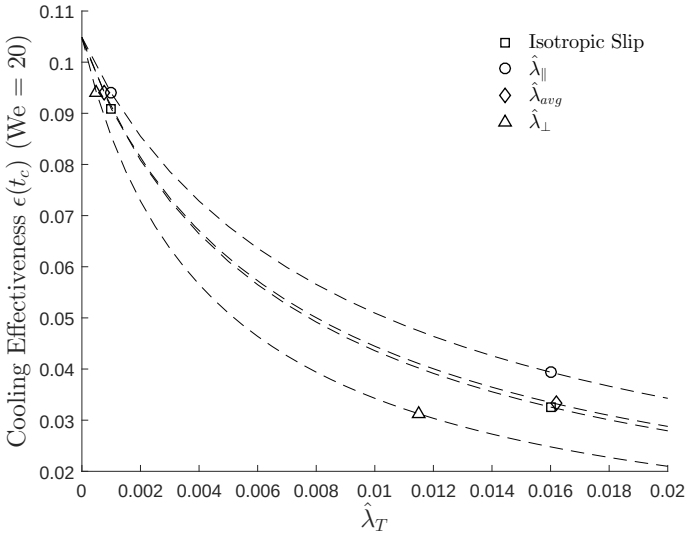

FIGURE 7. Comparison between isotropic and anistropic slip SH surfaces using different slip length reference points for the anisotropic SH surface. The Weber number was 20 and the contact angle for all slip lengths was held at 120 degrees.

surface there are multiple options for points of comparison. The first is to compare an anisotropic surface where the slip in the direction parallel to the ribs, $\lambda_\parallel$, is the same as the isotropic surface. The next is to ensure the slip in the perpendicular direction, $\lambda_\perp$, is the same. The third is to ensure that the average slip, λ_{avg}, is the same where

$$\lambda_{avg} = \int_0^{90} \lambda(\phi)\, d\phi \approx 0.77098\lambda_\parallel \tag{32}$$

The total cooling effectiveness for an isotropic surface is compared to an anisotropic SH surface when referenced by the parallel, perpendicular, and average slips for 4 different Weber numbers in Figures 7, 8, 9, and 10. These clearly demonstrate that across all Weber numbers considered that an anisotropic surface has approximately the same cooling effectiveness as an isotropic surface with a slip equal to its average slip. This is useful because it means that the simpler, isotropic model can be used even for anistropic surfaces by using the average slip length which reduces computation time and implementation complexity.

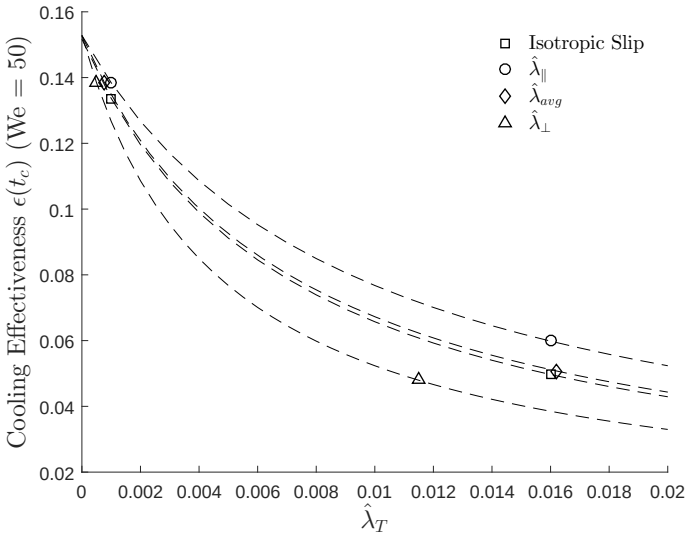

FIGURE 8. Comparison between isotropic and anistropic slip SH surfaces using different slip length reference points for the anisotropic SH surface. The Weber number was 50 and the contact angle for all slip lengths was held at 120 degrees.

CONCLUSIONS

The analytical model developed to predict the heat transfer to an impinging droplet can be useful for quickly evaluating the overall heat transfer to an impinging drop for a wide range of impact conditions and surface properties. The hydrodynamic model developed by Clavijo *et al.* used to evaluate the contact area as a function of time allows for the inclusion of the slip length as a parameter in the model [8]. The heat flux at the wall was predicted

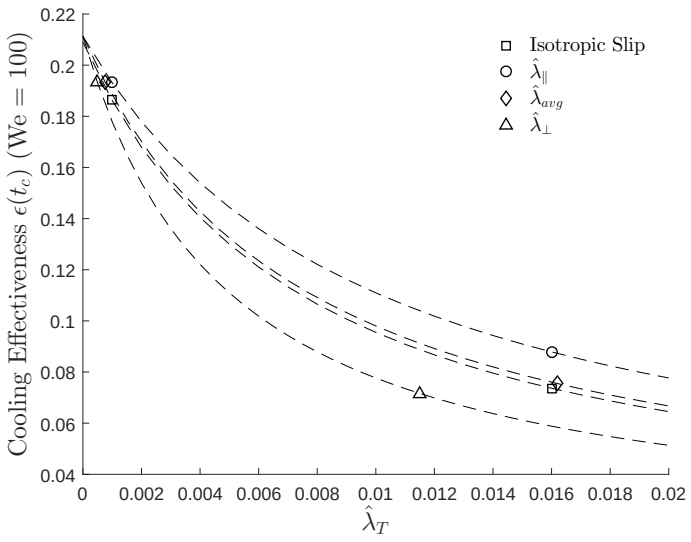

FIGURE 9. Comparison between isotropic and anistropic slip SH surfaces using different slip length reference points for the anisotropic SH surface. The Weber number was 100 and the contact angle for all slip lengths was held at 120 degrees.

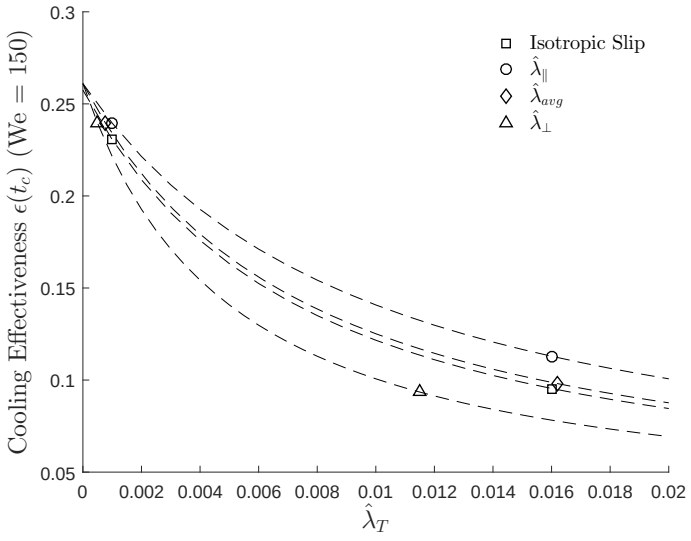

FIGURE 10. Comparison between isotropic and anistropic slip SH surfaces using different slip length reference points for the anisotropic SH surface. The Weber number was 150 and the contact angle for all slip lengths was held at 120 degrees.

using an integral method on the convection-diffusion equation. The convection term was resolved using four different velocity profiles and compared for goodness, with the Roisman profile producing the most accurate results.

Using the Roisman velocity profile to evaluate the convection term, the effect of contact angle, temperature jump length, and Weber number was explored. The cooling effectiveness decreased significantly with increasing temperature jump length as expected for all Weber numbers evaluated.

ACKNOWLEDGMENT

This work was supported by the Utah NASA Space Grant Consortium.

REFERENCES

[1] PasandidehFard, M., Qiao, Y. M., Chandra, S., and Mostaghimi, J., 1996. "Capillary effects during droplet impact on a solid surface". *Physics of Fluids,* **8**(3), pp. 650–659.

[2] Strotos, G., Gavaises, M., Theodorakakos, A., and Bergeles, G., 2008. "Numerical investigation of the cooling effectiveness of a droplet impinging on a heated surface". *International Journal of Heat and Mass Transfer,* **51**(19), pp. 4728 – 4742.

[3] Pasandideh-Fard, M., Aziz, S., Chandra, S., and Mostaghimi, J., 2001. "Cooling effectiveness of a water drop impinging on a hot surface". *International Journal of Heat and Fluid Flow,* **22**(2), pp. 201 – 210.

[4] Strotos, G., Aleksis, G., Gavaises, M., Nikas, K.-S., Nikolopoulos, N., and Theodorakakos, A., 2011. "Non-dimensionalisation parameters for predicting the cooling effectiveness of droplets impinging on moderate temperature solid surfaces". *International Journal of Thermal Sciences,* **50**(5), pp. 698 – 711.

[5] Strotos, G., Nikolopoulos, N., Nikas, K.-S., and Moustris, K., 2013. "Cooling effectiveness of droplets at low weber numbers: Effect of temperature". *International Journal of Thermal Sciences,* **72**, pp. 60 – 72.

[6] White, F. M., 2006. *Viscous Fluid Flow*, third ed. McGraw-Hill.

[7] ROISMAN, I. V., 2010. "Fast forced liquid film spreading on a substrate: flow, heat transfer and phase transition". *Journal of Fluid Mechanics,* **656**, p. 189204.

[8] Clavijo, C. E., Crockett, J., and Maynes, D., 2015. "Effects of isotropic and anisotropic slip on droplet impingement on a superhydrophobic surface". *Physics of Fluids,* **27**(12), p. 122104.

[9] Attan, P., Girard, F., and Morin, V., 2007. "An energy balance approach of the dynamics of drop impact on a solid surface". *Physics of Fluids,* **19**(1), p. 012101.

[10] Guo, C., Maynes, D., Crockett, J., and Zhao, D., 2019. "Heat transfer to bouncing droplets on superhydrophobic

surfaces". *International Journal of Heat and Mass Transfer,* **137**, pp. 857 – 867.

[11] Lauga, E., and Stone, H. A., 2003. "Effective slip in pressure-driven stokes flow". *Journal of Fluid Mechanics,* **489**, 6, pp. 55–77.

[12] Crowdy, D., 2011. "Frictional slip lengths for unidirectional superhydrophobic grooved surfaces". *Physics of Fluids,* **23**(7), p. 072001.

[13] Searle, M., Maynes, D., and Crockett, J., 2017. "Thermal transport due to liquid jet impingement on superhydrophobic surfaces with isotropic slip". *International Journal of Heat and Mass Transfer,* **110**, pp. 680 – 691.

[14] Cowley, A., Maynes, D., and Crockett, J., 2016. "Inertial effects on thermal transport in superhydrophobic microchannels". *International Journal of Heat and Mass Transfer,* **101**, pp. 121 – 132.

[15] Hays, R., Crockett, J., Maynes, D., and Webb, B. W., 2013. "Thermal transport to sessile droplets on superhydrophobic surfaces with rib and cavity features". In Proceedings of the ASME 2013 International Mechanical Engineering Congress and Exposition, no. IMECE2013-63780.